UNIVERSITY OF EXETER

I2 Individual Report

Experimental Wind Tunnel Testing for Comparison with CFD Simulation

DAVID DOCHERTY

2014

ECMM102

4th Year MEng Group Project

I certify that all material in this thesis that is not my own work has been identified and that no material has been included for which a degree has previously been conferred on me.

Signed……...

College of Engineering, Mathematics, and Physical Sciences
University of Exeter

Experimental Wind Tunnel Testing for Comparison with CFD Simulation

Individual Report-I2

2014

David Docherty
Candidate Number: 013545
Student Number: 600007039
Supervisor: Dr Gavin Tabor

Abstract

Aerodynamic design is important in the automotive sector as the aerodynamics of a car affect its performance (eg, fuel consumption, stability etc.). Wind tunnels are used to test the aerodynamic properties of a car during its design stage. Using ‘virtual’ wind tunnels to support physical wind tunnel tests could streamline the design process reducing the lead time of a design project and producing a better performing car. This report describes part of a project to investigate the use of computational fluid dynamics (CFD) in the aerodynamic design process. Specifically it describes the process of taking physical experimental results to be compared with results gained in ‘virtual’ wind tunnels, as a method of validating the CFD.

To perform experimentation a test section was designed and built for an open-circuit wind tunnel. This was used to find the drag coefficient of a concept car. These tests gave a drag coefficient of 0.17 ± 0.015, this was compared with other methods of measuring drag coefficient (alternative experimentation and CFD analysis). The report also presents a brief sustainability study regarding automotive drag force and physical vs computational energy consumption.

Keywords: Wind tunnel, test section, drag balance, coefficient of drag

Contents

1 Introduction

The automotive industry uses wind tunnels to test the aerodynamic properties of their cars as part of the design process. By using ‘virtual wind tunnels’ (models of wind tunnels using computational fluid dynamics) in parallel to physical wind tunnel testing, automotive companies could perform many more tests on their cars, and even test many iterations of their designs before taking it to full scale wind tunnel tests. This could decrease the cost of car development and improve the designs. This project explores the validity of using virtual wind tunnels in the automotive industry and addresses some of the issues associated with their use.

To investigate their use in the automotive industry, various ‘virtual wind tunnels’ would be designed using different computational fluid dynamics (CFD) simulations (RANS, LES, DES etc.). To validate these virtual wind tunnels, a concept car would be tested virtually and experimentally. The results of these tests would be compared to see how closely the ‘virtual wind tunnels’ resembled the real one. The main aims of this project were as follows:

- To co-design and manufacture a new test section for an open-circuit wind tunnel. Specifically to design and build a drag balance system.
- To use the drag balance to determine the coefficient of drag of a concept car.
- To analyse how this drag coefficient compares to drag coefficients found virtually using computational fluid dynamics (CFD), and use this comparison to develop conclusions about how CFD and practical experimentation can best be used for car design.

The wind tunnel used for the experimentation was an open-circuit wind tunnel described in section 2, along with more background information about why drag is an important quantity in the automotive sector and a review of previous experimental testing conducted. The test section of the wind tunnel had to be redesigned to improve the quality of experimental results, details of the new design are given in section 3. A description of the experimentation and results are given in section 4 prior to a discussion of the project’s sustainability in section 5. Suggestions for future improvements to the wind tunnel are given in section 6 and the report is concluded in section 7.

2 Background

Wind tunnels are used in the automotive industry to test the aerodynamic properties of cars. In general, car companies are interested in testing how their cars behave when moving through still air, the most common way of doing this is to use a wind tunnel. The aerodynamic properties of a car are related to the relative motion of it and the air around it, therefore a car moving through still air is equivalent to air moving across a stationary car. This is why wind tunnels are an effective way of measuring aerodynamic properties, it is far easier to mount instrumentation to a wind tunnel than to a moving car.

This section describes the basics of how wind tunnels are designed, then shows where these features are found in the actual wind tunnel used for testing in this project. It also describes why drag is important in the automotive industry, and presents details of previous experimentation conducted.

2.1 Wind Tunnel Design

Wind tunnels tend to be made from four basic components listed and described below:

1. **The Effuser:** Placed upstream of the model being tested, the effuser is where the air is accelerated from rest to the conditions experienced in the working section.
2. **The Working Section:** Also known as the test section, this is where the model is placed and where the measurements are taken. This report specifically deals with 'closed throat' wind tunnels meaning the working section is bounded by solid walls.
3. **The Diffuser:** This is designed to convert the kinetic energy of the air at the exit of the working section into pressure energy such that in theory with no losses a steady flow would continue.
4. **The Driving Unit:** In practise the losses in the system and the fact that the diffuser will not convert all the kinetic energy of the air, mean that the wind tunnel needs an addition of energy to ensure a continuous flow, the driving unit provides this. This is often supplied via a fan attached to an electric motor.

The location of the above features in an open-circuit wind tunnel are shown in the diagram in figure 2.1. An open circuit wind tunnel is the type used for testing throughout this report.

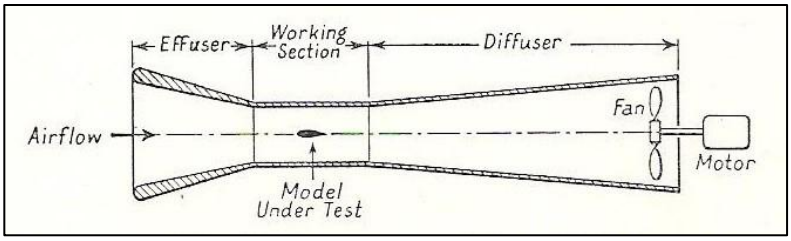

Figure 2.1: Cross-section of an open-circuit wind tunnel [1].

2.1.1 The Test Wind Tunnel

The wind tunnel used for the experimentation is an open circuit wind tunnel, similar to the diagram in figure 2.1. Figure 2.2 shows a picture of the wind tunnel with the various features labelled.

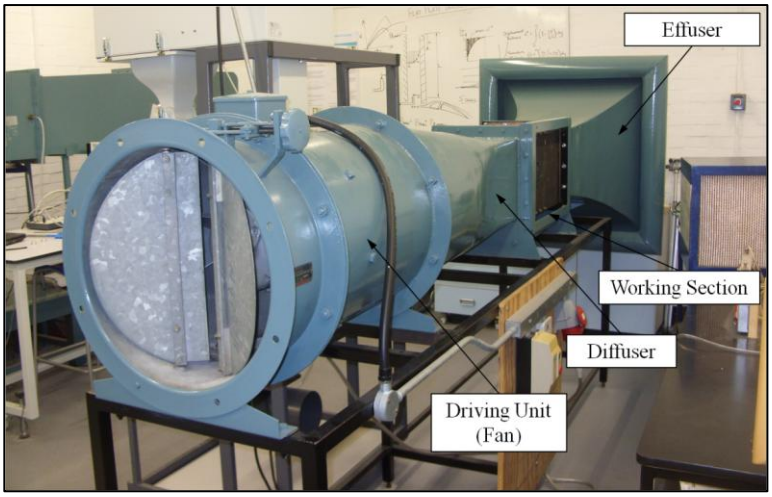

Figure 2.2: The wind tunnel used for experimentation[2].

The main issue with this wind tunnel was the test section. The test section was very basic in its design, it consisted of four PMMA (usually known by its trade name Perspex [3]) walls with various holes where instruments could be fed in. There were only limited tests which could be done in this test section, for example it didn't have a drag balance so drag had to be inferred from measuring velocities in an objects wake and using Von Karmen integral techniques [2].

Therefore the main aspect of this part of the project was to redesign the test section of the wind tunnel to improve the quality of the results for comparison with the CFD simulations. One part of this was to design a drag balance, section 2.2 goes into more detail about why drag is an important force in the automotive industry.

2.2 Drag Force in the Automotive Industry

The drag force on a car influences its performance, for example its top speed and most importantly its fuel consumption. Fears over cars' contribution to climate change mean that the reduction of fuel consumption is currently a major issue in automobile development. For example, the EU has recently set targets to increase the fuel consumption of the fleet average to 5.6 litres per 100km (42 miles per gallon) by 2015 and 4.1 l/100km (57.4mpg) by 2021 for petrol cars [4]. The fleet average describes the average fuel consumption across a manufacturer's whole range of cars.

The drag on a car is influenced by internal factors (friction in the engine, bearings, axles etc.) and external factors. The biggest external factor is air resistance [5] (drag) which plays a large role in the fuel consumption of a car. For example figure 2.3 shows the horsepower needed to overcome internal factors (blue) and aerodynamic drag (red) for a typical class-8 tractor trailer (a truck with a gross vehicle weight rating above 14969kg).

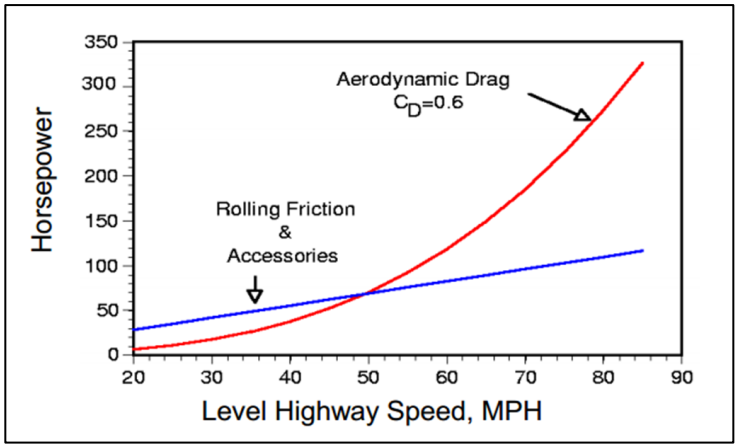

Figure 2.3: The effect of different sources of resistance at different speeds[6].

The graph shows that at low speeds the internal factors are the dominant sources of resistance, however as the vehicle moves faster (over 50miles per hour) the aerodynamic drag becomes the greatest source of overall drag.

Aerodynamic drag is the sum of two components; the pressure drag and the skin friction drag [7]. Normally these two effects can be considered together in an overall drag coefficient. The drag coefficient is dependent on the shape of the object and the Reynold's number of the flow[8]. The drag coefficient is related to the drag force by equation 2.1, where F_d is the drag force, ρ is the density of the fluid, U is the free stream velocity of the fluid and A is the frontal area of the object.

$$C_d = \frac{F_d}{0.5 \times \rho U^2 A} \quad (equation\ 2.1\ [7])$$

Typically the drag coefficient of a car is around 0.3. For example the bestselling car of 2013, the Ford Fiesta [9], has a drag coefficient of 0.33 [10]. A change in the drag coefficient of a car will have a direct affect on its fuel consumption. Equation 2.2 shows the relationship between the fuel consumption and the drag coefficient; where FC is fuel consumption, η is a property of the driving cycle (η≈0.5-0.7 for a car or truck at highway speeds), C_d is the drag coefficient, A is the frontal area and U is the speed of the vehicle.

$$\frac{\Delta FC}{FC} = \eta \times \left(\frac{\Delta C_d}{C_d} + \frac{\Delta A}{A} + \frac{3\Delta U}{U}\right) \quad (equation\ 2.2\ [6])$$

This shows that the fuel consumption can be increased by; reducing the speed at which the vehicle travels, meaning new speed limits would have to be instated on public roads, by reducing the frontal area of the car, which could reduce the room inside for passengers, or by reducing the coefficient of drag. The relationship between aerodynamic drag and a car's fuel consumption, combined with the pressure on car companies to be more environmentally aware, mean that the drag coefficient of a car is a key design criteria and even a selling point. To find the coefficient of drag the drag force at a particular air speed needs to be found experimentally, therefore most wind tunnels are fitted with drag balances to measure the drag force on a car. Given that one key output of the CFD simulations is a drag coefficient it is important that this can be measured experimentally, to do this a drag balance had to be designed and built within the new test section. Further detail of the drag balance as well as the test section design as a whole is presented in section 3.

2.3 Previous Wind Tunnel Testing

This section presents a brief summary of some initial testing performed in the old wind tunnel test section (for more detail see Docherty [2]). This wind tunnel testing was performed to gain a better understanding of the experimental method, it informed the design of the new test section.

The experimentation performed in the old test section was to find the drag force on a cylinder in cross flow by measuring velocities in its wake. A 48mm diameter cylinder was placed vertically in the wind tunnel, perpendicular to the flow. A hot-wire anemometer was used to measure the velocity of the air flow, this probe could be moved in one dimension horizontally behind the cylinder (y-axis). Due to the length of the probe a survey could only be conducted of half the wake behind the cylinder, the assumption was made that the wake would be symmetrical.

The drag force could be found by calculating the momentum loss in the flow from equation 2.3; where D is the drag force, L is the length of the cylinder, ρ is the density of air, b is the width of the wake, U_∞ is the free stream velocity and u_x is the measured velocity.

$$D = L\rho \int_0^b u_x(U_\infty - u_x)dy \quad (Equation\ 2.3\ [11])$$

Equation 2.3 is the Von Karmen Integral formula, in this case the measurements were not taken at infinitesimally small points but discrete points 5 mm apart across the wake of the cylinder. Therefore a discretised version of the Von Karmen integral formula was used, shown in equation 2.4 below:

$$D = L\rho \sum u_x(U_\infty - u_x)\Delta y \quad (Equation\ 2.4)$$

The velocity of the air was measured at 5mm increments across the wake of the flow, from the centre of the cylinder outwards, giving a velocity profile in the wake of the cylinder. Figure 2.4 shows a graph of these results.

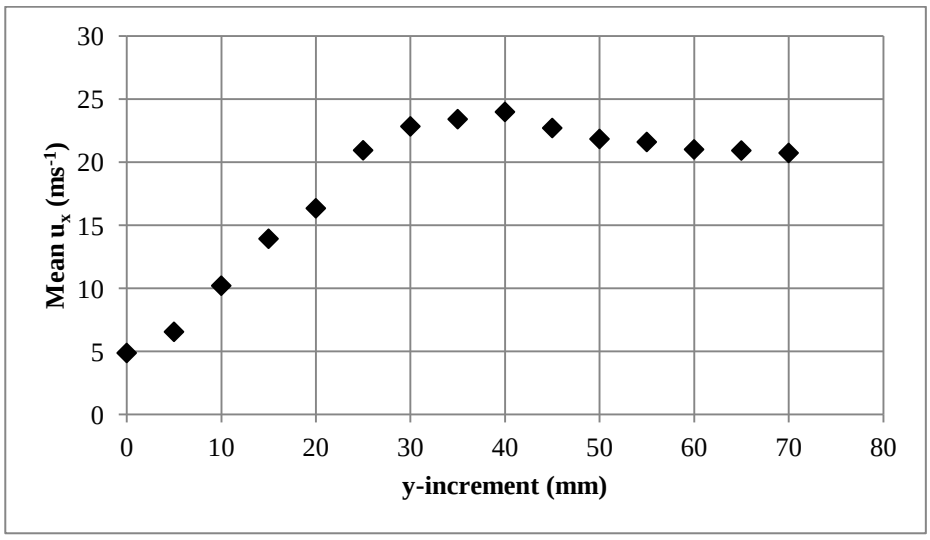

Figure 2.4: the velocity profile of the wake behind the cylinder [2].

Figure 2.4 shows how the velocity of the air directly behind the cylinder is at a minimum and increases as the probe moves outwards until it reaches the free stream velocity of 21.84ms^{-1}. By substituting this data into equation 2.4 a drag force was found of 1.63N. The drag force on the cylinder was also calculated based on previous experimental data to be 4.13N. More details about these results and their comparison to theoretical values can be found in Docherty [2].

The difficulties found in this experimentation informed the specifications used to design the new wind tunnel test section, some of these difficulties are outlined below:

- **Probe manoeuvrability:** In this case the hot wire anemometer could only be moved in one dimension (the y-axis), this was fine in this instance as the object being tested was prismatic. However in order to test the wake of a concept car using the same method, measurements would have to be taken in at least two dimensions behind the car. The new test section would require a method for moving a probe in at least two dimensions (ideally three) in the flow.
- **Experimental setup:** The design of the wind tunnel test section made the setup of experiments very difficult, only the back half of the test section could be properly accessed by removing a panel. There were also multiple holes and gaps in the walls of the wind tunnel which had to be filled prior to testing. The new test section would benefit from giving its users more room to setup their experiments, having a whole removable wall for example would be very helpful.
- **Visibility:** Whilst the walls of the wind tunnel were made from clear Perspex, they had been scratched and scuffed in time such that visualising what was happening inside the wind tunnel was very difficult. The new test section would benefit from having more clear surfaces made from a harder material, more resistant to scratches.

3 Test Section Design

This section describes the design of the new test section, it describes the process used and gives reasons for the design decisions made. Firstly, section 3.1 details the overall design of the test section before the design of the drag balance is given in more detail in section 3.2. The various force measurement options for the drag balance are discussed and compared in section 3.3.

3.1 Overall Test Section Design

The overall design of the test section was generated by an iterative process and governed by some key specifications, these were developed from experience gained from working with the previous test section. The main specifications of the design of the test section were that it had to:

- Mount into existing open-circuit wind tunnel.
- Have minimal intrusion into flow (the cross section should be a 305mm square).
- Include a drag balance.
- Include a mechanism for moving a probe within the test section.
- Allow a good overall view of the interior of the wind tunnel to aid future work into flow visualisation.

These specifications led to the design shown in figure 3.1.

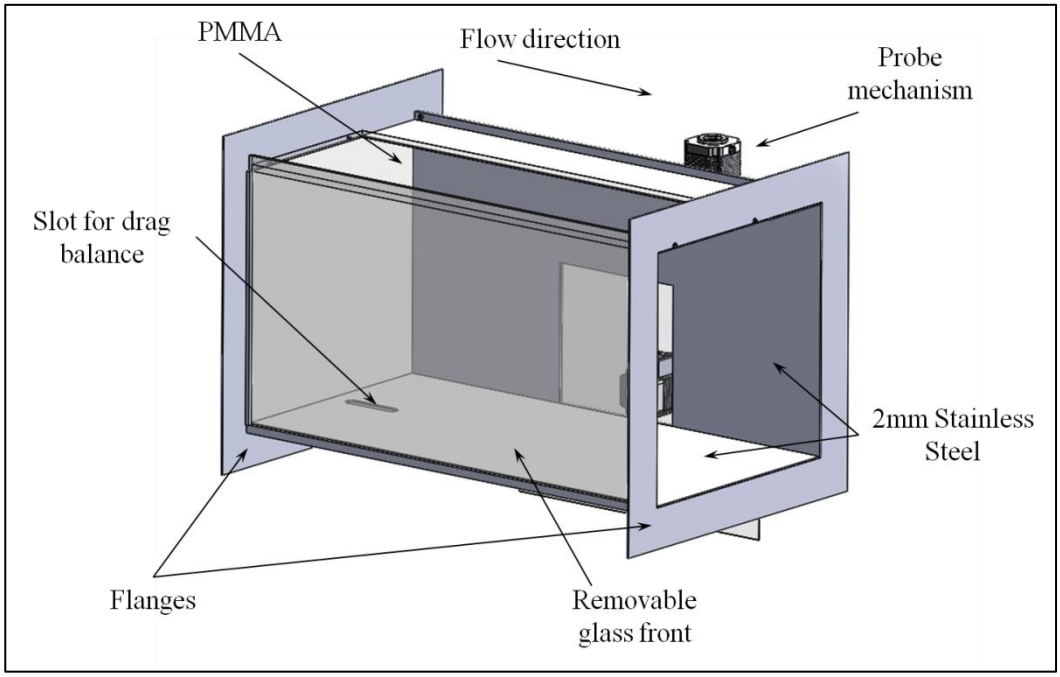

Figure 3.1: The overall design of the test section.

The bottom and back panels of the test section are made from 2mm thick stainless steel welded to each other and the stainless steel flanges at either end. The flanges have holes drilled in them so the test section can be bolted in place. The mechanism to move the probe is mounted on the back panel, described in more detail in Blades [12].

The top panel is made up of a small stainless steel strip and a large Perspex panel screwed into the flanges. This Perpsex window along with the glass front of the test section

gives a clear view of what is happening in the wind tunnel. The glass panel at the front is entirely removable allowing for easy access to set up experiments before replacing the panel and running them. There is a slot cut in the bottom panel of the test section, this is to accommodate the drag balance design discussed further in section 3.2.

3.2 Drag Balance Design

This section briefly describes the design process used for the drag balance. The final drag balance is then presented and described in detail. This drag balance would be manufactured and used to find the drag coefficient of the concept car experimentally.

3.2.1 Design Process

The first part of the design process was to determine the specifications that the design had to meet, they are presented and explained below.

- **Accuracy of results**: The primary purpose of the drag balance is to give accurate results of drag force, from which the drag coefficient can be calculated. Therefore the drag balance should have a low internal friction, reducing the error of the results obtained. This also includes that it should be as unobtrusive to the flow as possible.
- **Versatility**: The drag balance should be capable of using a variety of force meters to measure the drag force, this is a method of improving the accuracy of the results. It should also be versatile in the sense that it can be fitted to different types of model allowing the drag balance to be used for many future applications.
- **Durability**: The test section should be designed for future use beyond the goals of this particular project. Therefore the drag balance should be simple and durable to accommodate many future tests.
- **Ease of manufacture**: The time scale for the project was limited, and given that the drag balance had to be manufactured alongside the rest of the wind tunnel test section ideally the drag balance should be as simple to build as possible. This would free up time to be used to manufacture other parts and leaves time at the end to perform multiple tests.

These specifications informed four concept designs shown in figure 3.2. These designs were compared in a matrix analysis [2] and informed the final design in section 3.2.2.

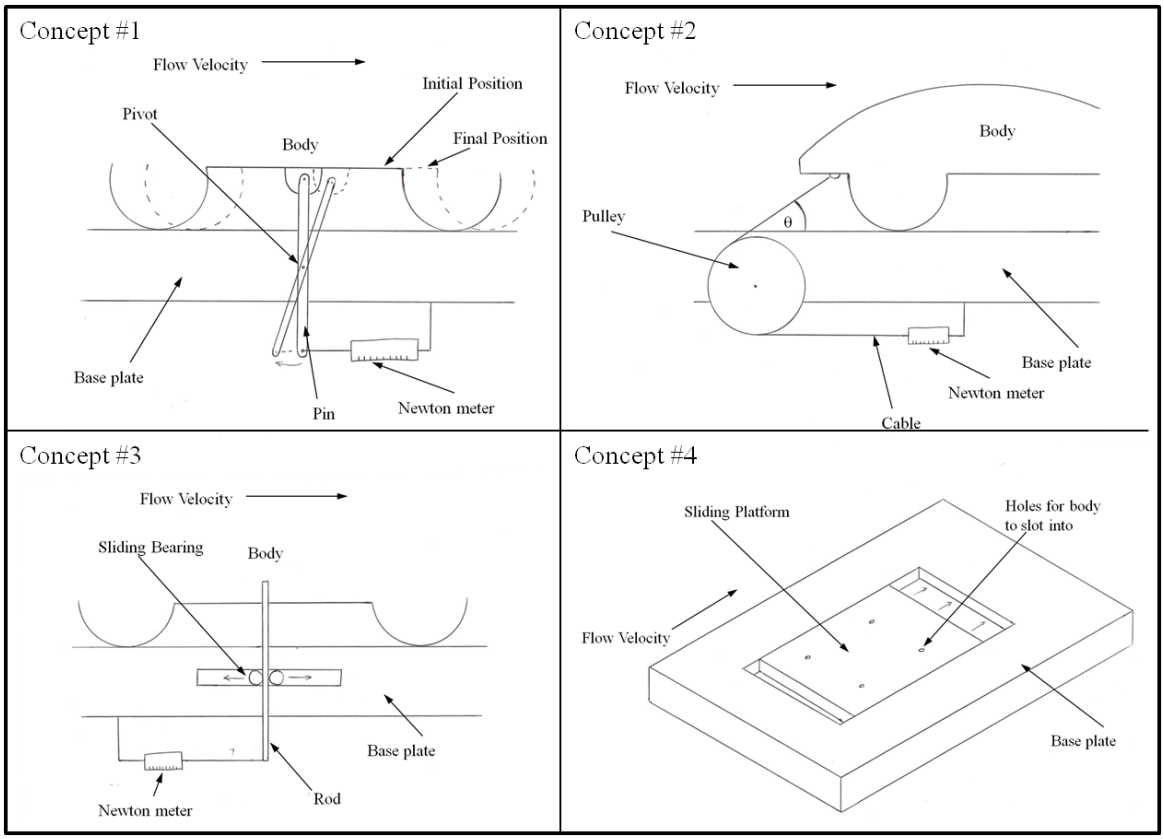

Figure 3.2: The four drag balance concept designs [2].

3.2.2 Final Design

The matrix analysis showed that the second concept was one of the strongest designs and met the specifications. It was therefore developed into the final design shown in figures 3.3 and 3.4.

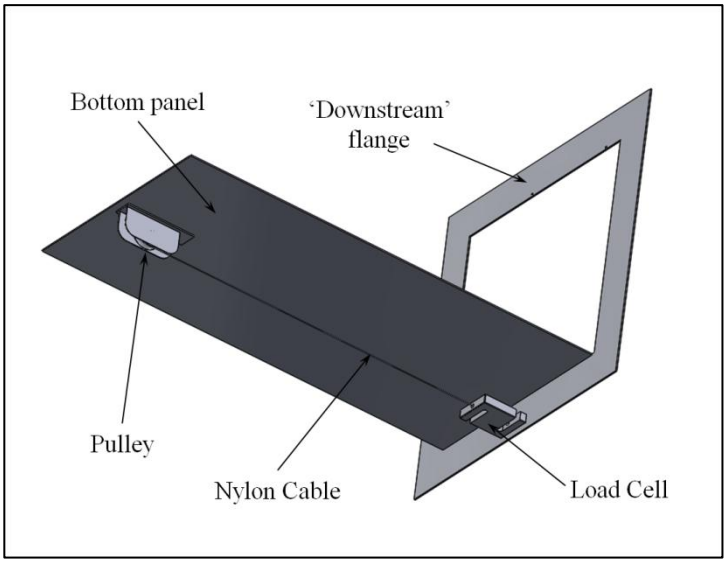

Figure 3.3: The drag balance design viewed from below.

The drag balance is formed of a cable attached at one end to a load cell and the other to the model in the wind tunnel via a pulley in the base of the test section. The load cell is bolted to the flange and the pulley's stainless steel casing is welded to the bottom panel

beneath the slot shown in figure 3.1. Figure 3.4 shows the design in more detail from the front and side views.

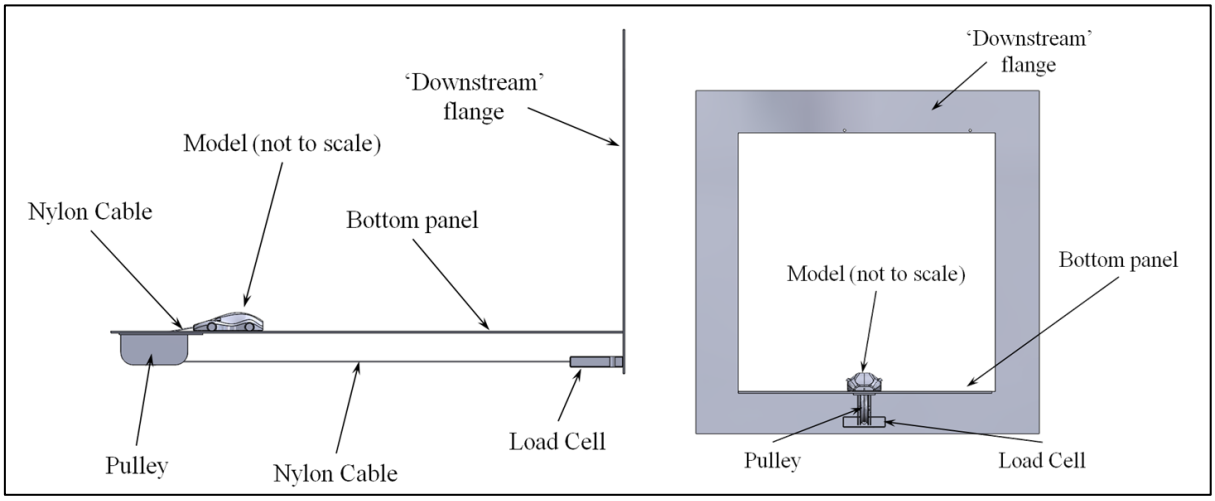

Figure 3.4: The drag balance design side (left) and front (right) views.

The drag balance works by balancing the drag force on the model with the tension in the cable. The tension in the cable is measured by a load cell. An important aspect of this design is to take note of the angle of the cable within the wind tunnel, the results found by the load cell need to be adjusted trigonometrically to give the true drag force. One advantage of this design is the versatility of force measurement methods, figures 3.3 and 3.4 show a load cell being used, however this can be replaced by a simple force meter (eg. a spring Newton meter) or other force measurement devices. The various options for force measurement are described in section 3.3.

3.3 Force Measurement

This section describes the various options for force measurement within the drag balance design. For each option the advantages and disadvantages are stated along with a description of how they operate, these options are then compared in a matrix analysis in section 3.3.5. The main considerations made for the choice of force measurement were:

- **Accuracy and Precision**: For the experimental testing the results had to be as accurate as possible, meaning that the meter used to measure the force had to have the highest accuracy possible. The precision of the meter is also important, small fluctuations in the drag force could affect the accuracy of the drag coefficient.
- **Cost:** The budget for the project as a whole was limited and there were other areas of the project where more money had to be spent, for example the probe moving mechanism [12]. Therefore the choice of force measurement had to be as cost effective as possible.
- **Ease of implementation**: The force meter should be quick to implement into the design described in section 3.2.2, the time scale of this project was limited so any saving in time would leave more time for experimentation and other aspects of test section manufacture.
- **Durability:** The force meter should be durable so that the drag balance can be used for future experimentation.

3.3.1 Spring Newton Meter

A spring Newton meter simply works by measuring the extension of a spring from an applied force. As long as a spring remains within its elastic region it obeys Hooke's law, meaning the applied force is directly proportional to the extension of the spring. Equation 3.1 shows how force is related to extension.

$$F = -kx \ (Equation\ 3.1) \ [13]$$

Where F is the applied force (N), x is the extension of the spring (m) and k is the spring constant or the 'stiffness' of the spring (Nm^{-1}). Therefore by measuring the extension of a spring the applied load can be inferred. Figure 3.5 shows an example of a spring Newton meter.

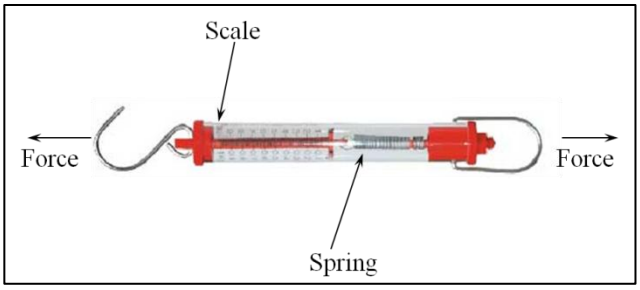

Figure 3.5: A spring Newton meter [14].

The advantage of using a spring Newton meter is that they are very cheap, reliable and they do not require software to run. They are accurate and can be purchased in various levels of precision (tend to be around ± 0.25N), however they are read by human observation and so readings must take into account human based errors such as parallax error. The readings may also fluctuate with time and spring Newton meters cannot be used in conjunction with data loggers to get time averaged results.

3.3.2 Load Cell

Load cells are force sensors which are hydraulic, pneumatic or strain gauge based. Strain gauge based load cells are the most common type [15] . This section first describes how strain gauges operate and then explains how they are used in load cells.

Electrical resistance strain gauges (known commonly as strain gauges) infer the strain of a material from a change in resistance. They are formed of a 'zig-zagging' conductor on a thin polymer film. At either end of the conductor is a solder tab, to which wires can be soldered. Figure 3.6 shows a diagram of a typical strain gauge.

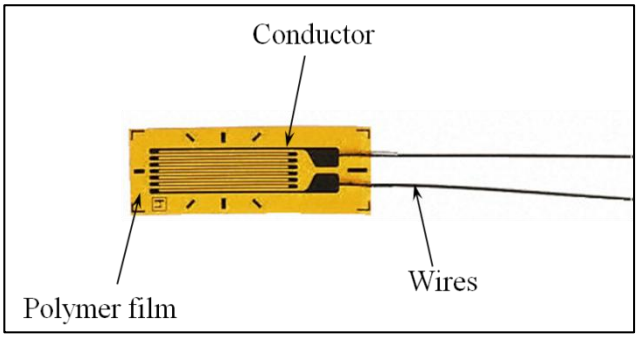

Figure 3.6: A typical electrical resistance strain gauge [16].

The strain gauge is glued to the surface of whatever is being measured such that as the material strains the gauge strains by the same amount. As this happens three changes occur in the conductor; the length, the cross-section and the specific resistivity [17]. These three changes result in a difference in resistance of the conductor, this difference in resistance is directly proportional to the strain experienced by the strain gauge, equation 3.2 shows the relationship between the change in resistance and the strain.

$$\varepsilon = \frac{dR/R}{G_f} \quad (equation\ 3.2)\ [18]$$

Where R is the resistance, ε is the strain and G_f is the 'gauge factor' (sensitivity) of the strain gauge. Gauge factor varies but for most common strain gauges it is 2.1 (for alloys of 45% Nickel and 55% Copper) [19].

Four of these strain gauges are arranged in an s-beam load cell as shown in figure 3.7. Figure 3.7 shows a photograph of an s-beam load cell and a cross-section which details how the strain gauges are arranged. The four strain gauges are connected together in a Wheatstone bridge circuit. This circuit is used in many sensor electronics to compare changes in resistance. A more detailed description of the Wheatstone bridge is given in section 3.3.3.

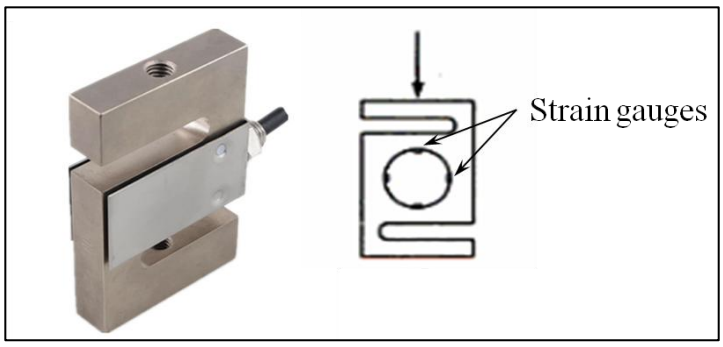

Figure 3.7: An s-beam strain gauge [20] (left) and a cross section showing the locations of the strain gauges [18] (right).

The advantages of load cells include that they can be used in conjunction with data loggers, this means that fluctuations in force can be measured and recorded in real time, this would be very difficult with spring Newton meter. The precision of a load cell is dependent on the data logger used, typically around 0.01N. Load cells remove the human error from the readings as they are taken directly from measuring voltage, they are also very robust and reliable. Load cells are however very expensive compared to the other methods of force measurement.

3.3.3 Beam type load cell

Making a force meter from strain gauges on a beam offers many of the advantages of the load cell but at a fraction of the cost. A beam type load cell is a very simple form of load cell, it is simple enough to be relatively easy to manufacture. A beam type load cell is formed of applying four linear strain gauges to a cantilever beam as shown in figure 3.8.

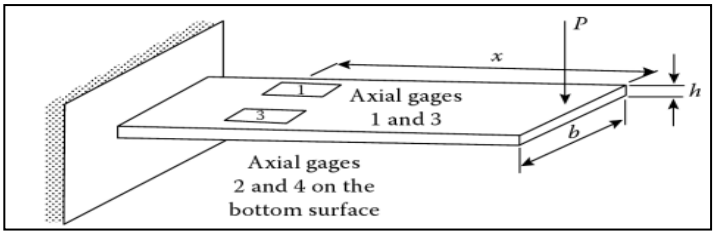

Figure 3.8: The arrangement of strain gauges on a beam type load cell [21].

These four strain gauges are connected into a Wheatstone bridge circuit as shown in figure 3.9.

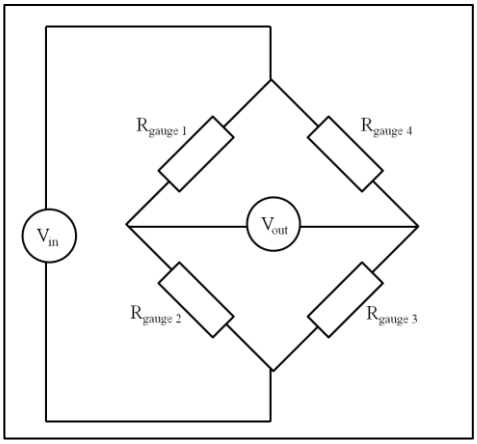

Figure 3.9: How the strain gauges are arranged in the Wheatstone bridge circuit.

The input voltage V_{in} is constant and as the resistance of the strain gauges change the output voltage V_{out} changes, this can be measured by a voltmeter and can be used with a data logger. This arrangement of strain gauges directly relates the output voltage to the applied load P, shown in equation 3.3.

$$P = \frac{V_{out}Ebh^2}{6V_{in}G_f x} \quad (equation\ 3.3)[21]$$

Where E is the Young's modulus of the beam material, G_f is the gauge factor of the strain gauges and b, h and x are the dimensions shown in figure 3.8. From equation 3.3, the load at the end of the beam can be inferred from measuring the output voltage of the circuit shown in figure 3.9. This output voltage can be used in conjunction with a data logger meaning variations in load can be measured and recorded in real time without introducing human errors such as parallax errors. Like the load cells the precision is dependent on the data logger used, typically around 0.01N. This option provides many of the advantages of a commercial load cell at a fraction of the cost but does offer slightly reduced accuracy.

3.3.4 Digital force meter

Another method of force measurement would be to use a digital force meter. These range significantly in price and accuracy but in principle work similarly to the beam type load cell. Figure 3.10 shows an example of the workings of a low end digital force meter. It consists of a strain gauge attached to a small beam which is fixed at either end to attachments. The force is applied to these attachments (left and right in figure 3.10), this bends the beam. The resistance of the strain gauge alters and is read by a Wheatstone bridge circuit and outputted as a force reading.

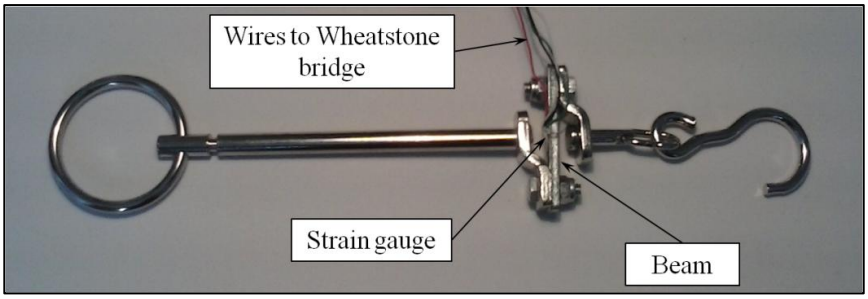

Figure 3.10: The workings of a simple digital force meter.

Digital force meters vary in their cost and accuracy, the low end force meters would be useful in this project as cost is a limiting factor in the drag balance design. A low end digital force meter operates similarly to a spring newton meter as it cannot be used in conjunction with a data logger. The process of reading these types of force meters is easier however due to their digital displays, this reduces the human error involved in taking the readings. Their precision varies depending on the model, however ±0.05N can be achieved even using low end digital force meters.

3.3.5 Force measurement comparison

To decide upon the best option or options for force measurement a matrix analysis was performed on the force measurement techniques described above, the matrix is shown in table 3.1. Each technique was graded out of 10 against criteria listed along the top of the table based on the information provided in sections 3.3.1 through 3.3.4, each criteria was given a weighting based on its relative importance. The grade was multiplied by the weighting which was then summed to give a total.

Table 3.1: Matrix analysis for comparison of force measurement techniques.

Force measurement technique	Accuracy	Precision	Cost	Ease of Implementation	Durability	Total
Weighting	**3**	**3**	**2**	**1**	**1**	
Spring Newton Meter	6	6	9	8	7	69
S-beam load cell	9	9	3	7	9	76
Beam type load cell	7	9	7	6	4	72
Digital force meter	6	7	9	8	8	73

The matrix analysis in table 3.1 shows that the best option for the force measurement is the s-beam load cell. In practise it was still too expensive to buy one new so a digital force meter was purchased for the purposes of the testing as the next best option. Later in the project an old unused piece of laboratory equipment was harvested for its working s-beam load cell. This meant that the testing could use two types of force measurement device and compare results. The experimental methodology is described in section 4.

4 Experimentation

This section describes how the experimental results were achieved. It details some of the steps taken to ensure good health and safety and then goes on to explain some of the errors within the experiment and how they were minimised or taken into account. Finally the results are presented with a comparison to what was found in other wind tunnel tests and a CFD simulation.

4.1 Setup and Methodology

The wind tunnel test section as shown in section 3.1 was manufactured and installed to replace the old test section shown in figure 2.2. The new test section shown on the left in figure 4.1 contains a mechanism for moving a probe (pitot tube or hot-wire anemometer) freely in three dimensions. This mechanism is installed on the back panel and is described further in Blades [12]. It also has a removable glass panel in the front which allows for good visibility during testing. In the base of the test section is the drag balance mechanism, shown on the right in figure 4.1. The model concept car was manufactured by additive layer manufacturing (ALM) and filled with plaster, the ball bearing wheels minimise friction between the car and the surface of the test section to improve the accuracy of the results. Further details of the concept car manufacture are provided in Browne [22].

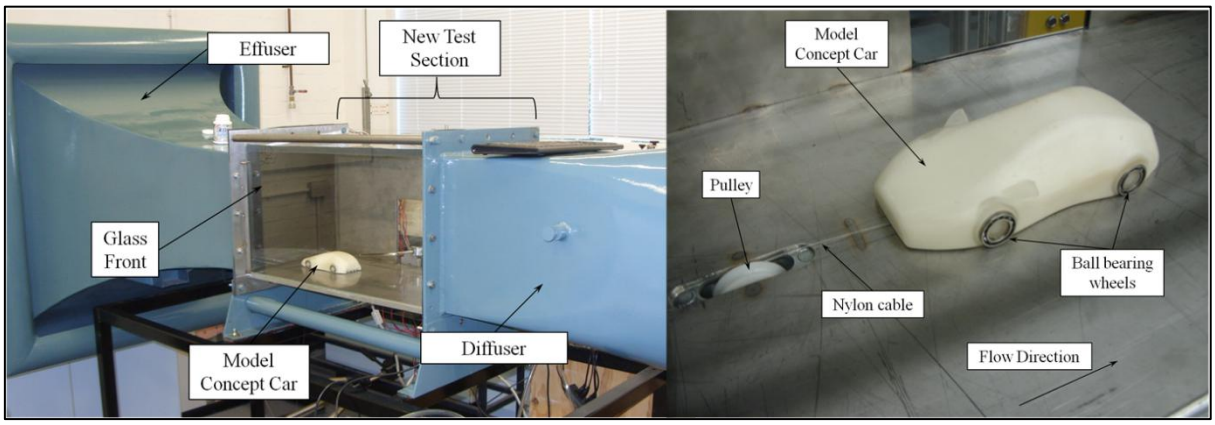

Figure 4.1: The new test section (left) and a close up of the drag balance mechanism (right).

The picture on the right of figure 4.1 shows the internal mechanism of the drag balance. A nylon cable is attached to the underside of the model concept car by epoxy resin. The cable goes through a pulley to a load cell/force meter mounted below.

To achieve accurate results two methods of force measurement were used on the underside of the drag balance for testing. The first was to use an s-beam load cell mounted to the flange below the test section. Figure 4.2 shows a side view of the drag balance and how the load cell was connected. The output of the load cell was connected to a data logger which displayed the applied load, it measured the load to a precision of 0.01N.

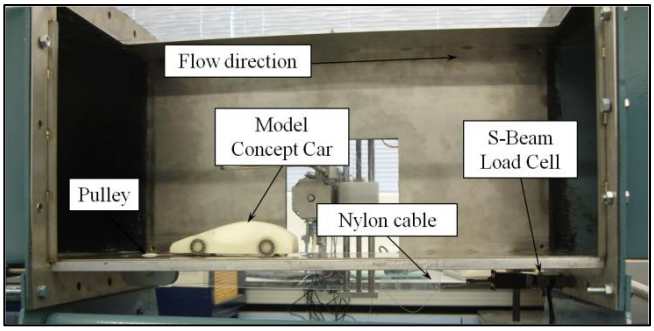

Figure 4.2: A side view of the drag balance showing the load cell.

The second method of force measurement was a simple digital force meter attached to a weight below the test section. Figure 4.3 shows how the force meter was attached. The force meter displays the load in kg to a precision of 0.01kg. By using these two force measurement methods in tandem a more accurate value for the coefficient of drag could be found.

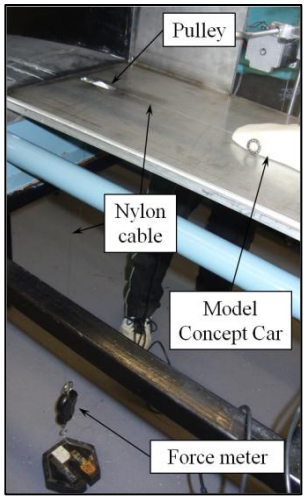

Figure 4.3: How the force meter was mounted below the test section.

The experimental method consisted of first attaching the load cell to the model and switching on the wind tunnel. Once the wind tunnel was up to speed (38.88ms^{-1}, found experimentally [12]) a reading was taken from the data logger. The readings remained steady and did not vary, it was therefore unnecessary to take time averaged values of force. It was also important to note what the data logger read when the wind tunnel was not switched on at the start and end of the testing to account for the zero error.

The nylon cable was then detached from the load cell and attached to the force meter as shown in figure 4.3. The test was repeated; switching the wind tunnel on and taking readings once it had reached its full speed. Again there was no fluctuation in the results so a time average was unnecessary. The results of this experimentation are presented in section 4.3 along with a comparison to what was found in CFD simulation.

4.1.1 Health and Safety Risk Assessment

The experimentation contained certain risks to health and safety. In order to limit these a risk assessment was performed as shown below in table 4.1. The risk assessment also contains hazards associated with the use of the workshop for the manufacture of the test section.

Table 4.1: The health and safety risk assessment for the experimentation and workshop use.

Hazard	Who does it affect?	Potential Consequence	Preventative Actions
Debris exiting the wind tunnel.	Experiment participants.	Physical harm. Damage to the wind tunnel.	• Remove any loose objects near the inlet. • Secure all objects in the wind tunnel. • Do not stand directly behind the outlet of the wind tunnel.
Trip hazard due to pipes, wires etc. associated with experimental equipment.	Experiment participants.	Physical harm. Damage to the wind tunnel. Could render results inaccurate.	• Avoid trailing cables or tubes if possible. • Keep the number of participants to a minimum.
High noise levels.	Experiment participants.	Hearing damage.	• Wear ear protection when the wind tunnel is switched on.
Workshop Accident	Those manufacturing the new working section.	Physical harm from tools, machinery etc.	• Wear personal protective equipment (PPE). • Secure work pieces appropriately.

4.2 Experimental Errors

In order for the results of the experiment to be accurate, associated errors must be assessed, reduced and taken into account where possible. This section describes some of the experimental errors found in this experimentation and how they were dealt with.

4.2.1 Measurement

The first important error to consider is the precision of the meters used for the tests. The load cell measures to a precision of 0.01N giving an error of ±0.005N. The force meter measures in kg to a precision of 0.01kg giving an error of ±0.005kg, this translates to an error of ±0.049N.

4.2.2 Angle of the cable

The angle of the cable must be taken into account to gain an accurate description of the drag force on the car. The tension in the cable must be adjusted for the angle at which it lies inside the wind tunnel, figure 4.4 shows the angle, θ.

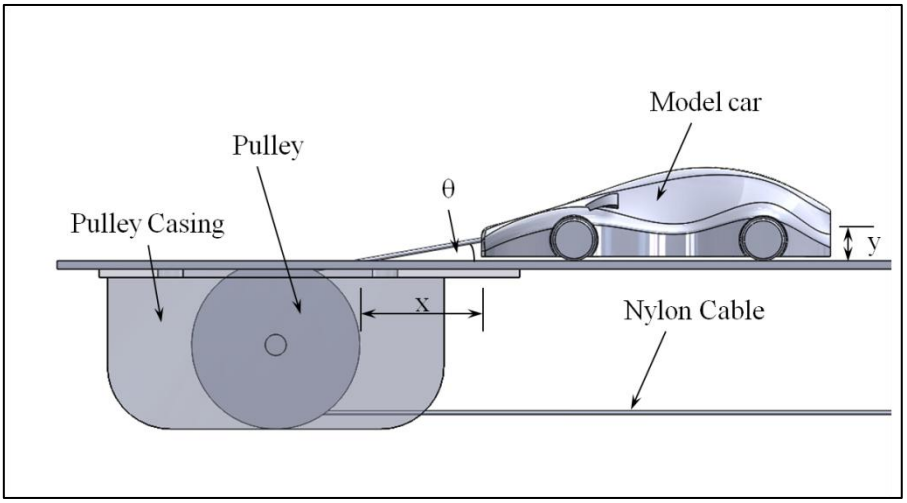

Figure 4.4: A side view showing the angle of the cable.

The angle θ is found by measuring the distances x and y using a ruler and using trigonometry: $\tan\theta = y/x$. In this case the car was so low (y=1.99mm) and far away from the pulley(x=290mm) that the angle was very small ($\theta = 0.39^{o}$). This angle is so small that its effect on the results is negligible.

4.2.3 Other Errors

Another experimental error is the frictional force within the pulley and the bearings. This frictional force would cause the measured drag force to be lower than the real one, therefore it was important to measure these forces.

The bearing friction was found by simply measuring the amount of force required to move the car from stationary, this was done using the digital force meter. It was found that the frictional force was lower than the precision of the instrumentation and therefore has a negligible effect on the results. This low frictional force is due to the bearings themselves having very little internal friction and the fact that the coefficient of friction between the bearings and the stainless steel of the wind tunnel is so low.

The friction in the pulley was found by using a force meter to apply a load to one end of the nylon cable and measuring the force at the other using another force meter. Any discrepancy between these results would be the frictional force within the pulley. Again in this case the frictional force was found to be lower than the precision of the instrumentation, meaning the friction in the pulley is negligible.

4.3 Results

The experimentation described above ($38.88ms^{-1}$ wind speed across the model car) lead to two values of drag force;

- Load cell reading: 0.49N ±0.005N
- Force meter reading: 0.39N ± 0.049N

A more useful value than drag force however is coefficient of drag, as given in equation 2.1. The coefficient of drag is a more useful quantity as it is a dimensionless value, meaning it will remain the same for different sizes of model tested at different speeds. Coefficient of drag is dependent on geometry and flow characteristics (eg. turbulent or laminar flow). The quantities required to find the coefficient of drag are as follows:

- Drag force (F_d): Found experimentally, given above.
- Flow velocity (U): Found experimentally, $38.88ms^{-1}$ [12].
- Density of air (ρ): 1.2027 kgm^{-3} at 20.5ºC [23].
- Frontal area (A): Found from CAD model as shown below.

The model concept car was manufactured by ALM, therefore an accurate method of measuring the frontal area was to extract it from the CAD model used. Figure 4.5 shows the CAD model of the concept car and the frontal area outlined in front of it. Given a shape, the 'measure' tool in Solidworks [24] can find its area. In this case the frontal area (A) of the model concept car used in the testing was $2932.92mm^2$.

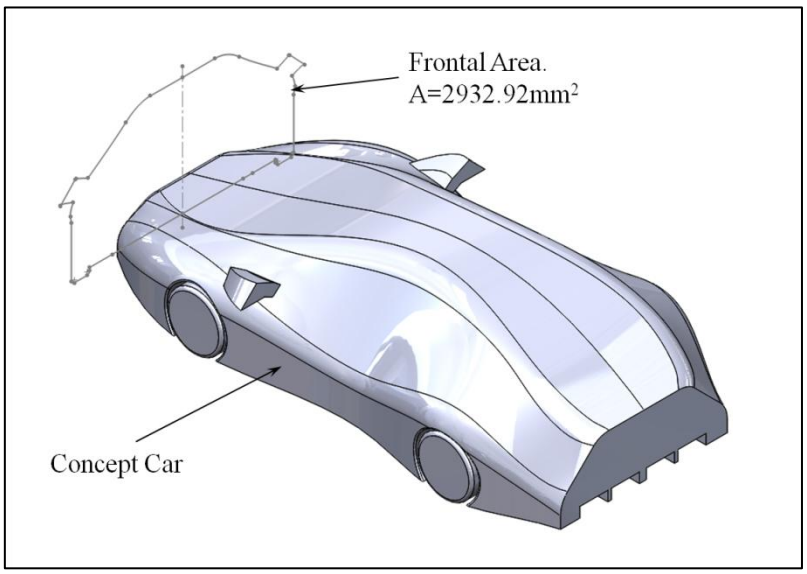

Figure 4.5: The CAD model of the concept car showing its frontal area.

By substituting these values into equation 2.1 two drag coefficients were found:

- $C_{d\ load\ cell} = 0.18 \pm 0.003$
- $C_{d\ force\ meter} = 0.15 \pm 0.027$

Taking the mean of these two values gives a coefficient of drag for the concept car of 0.17 ± 0.015. The coefficient of drag was also found from other methods, including a wake velocity survey [12] and a CFD simulation [25]. These results of drag coefficient are shown below in table 4.2.

Table 4.2: The various calculations of drag coefficient.

Method	Coefficient of Drag
Drag balance experimentation	0.17 ± 0.015
Wake velocity survey	0.35788 [12]
CFD simulation	0.167 [25]

4.4 Discussion and Analysis

The coefficient of drag found by the wake velocity survey is higher than that found by the drag balance experimentation. There are two main reasons for this; firstly the boundary layer was thinner for the wake velocity survey as the car was closer to the inlet (more details of boundary layers are given in section 4.4.1) and secondly the car was at a 14° angle to the streamwise direction explained in more detail in Blades [12]. The thicker boundary layer in the drag balance testing would decrease the drag force as the flow is moving slower overall, giving a lower drag coefficient. Similarly by placing the concept car at an angle to the flow the testing is not equivalent, a car is likely to have a lower drag force with the flow moving straight over it than at an angle, this is another reason for the drag coefficient from the drag balance experimentation to be lower than that found by the wake velocity survey.

A RANS CFD simulation was run in Fluent [26] to replicate the positioning and conditions of the drag balance testing, details of the specific setup is given in Nima [25]. This CFD simulation gave the coefficient of drag to be 0.167, this is well within the errors of the experimental technique giving more credence to the accuracy of the experimental results. The setup of this CFD testing had been previously validated by performing tests comparable to literature. This shows that a 'virtual wind tunnel' made using CFD is a valid equivalent to physical wind tunnel testing. In practise CFD can be used in conjunction with physical wind tunnel testing in the automotive design process. The advantages of using CFD are that it can test many different designs quickly, where they would each have to be physically modelled for wind tunnel tests, and that CFD can model many different flow and environmental conditions. For example CFD can model temperatures, weather and wind conditions which would be very costly to install in a physical wind tunnel. CFD therefore has the potential to lower the cost and lead time of an automotive design project.

Another good comparison for the experimental results would be to compare with a similar style car currently on the market. The best-selling saloon style car in 2013 was the BMW 3 series [9], which has a drag coefficient of 0.29 [27]. The drag coefficient of the concept car found experimentally is comparable to this, however it is lower for various reasons. Firstly, the cars have different geometries, an example of this is that the concept car is lower to the

road than the BMW, causing it to have a lower drag. Secondly, the concept car is just an external shell and doesn't contain any modelling of internal engine flow, the grill and engine cooling of the BMW would add to its drag force. Another reason would be the fundamental differences between wind tunnel testing and real world scenarios. Given that wind tunnel tests are designed to replicate a vehicle moving through still air it is important to understand how close these two cases are in practise. Sections 4.4.1 and 4.4.2 give some of the differences between a vehicle moving through still air and a model in a wind tunnel.

4.4.1 Boundary Layer Thickness

The boundary layer is the "region of fluid close to a surface immersed in a fluid flow" [7]. The fluid at the surface has the same velocity as the surface, the fluid far away from the surface is at the free stream velocity. The space in transition between these two velocities is the boundary layer.

When a vehicle moves through still air there is no boundary layer generated by the road surface. In the wind tunnel test describes in section 4.1 however there is a boundary layer generated by the surfaces of the test section. To find the thickness of the boundary layer the wind tunnel surfaces are modelled as a flat plate. To determine whether the boundary layer is laminar or turbulent the Reynold's number based on x (Re_x) must be found, if Re_x is greater than $5x10^5$ then the boundary layer is turbulent. The Reynold's number based on x is determined by equation 4.1, where U is the free stream velocity ($38.88ms^{-1}$), x is the distance from the front of the wind tunnel to the model (effuser length + distance from front of test section to model = 1.02m) and ν is the kinematic viscosity of air ($9.49x10^{-6}$ [28]).

$$Re_x = \frac{Ux}{\nu} \quad (equation\ 4.1[7])$$

Substituting the above values into equation 4.1 gives $Re_x=4.18x10^6$, therefore the boundary layer is turbulent and can be calculated from equation 4.2. Where δ is the boundary layer thickness (combined laminar and turbulent boundary layers), x is the distance from the front of the wind tunnel to the model and Re_x is the Reynold's number based on x.

$$\delta = \frac{0.382x}{Re_x^{0.2}} \quad (equation\ 4.2\ [29])$$

Substituting x and Re_x into equation 4.2 gives δ=18.5mm, roughly a third the height of the car model. This boundary layer would not be found in the case of a car moving through still air meaning that in the real world the drag coefficient is likely to be higher than that found experimentally.

4.4.2 Horizontal Buoyancy

The assumption made in wind tunnel testing of vehicles is that a body moving through still fluid is entirely equivalent to moving fluid over a still body. In practise however wind tunnels cannot replicate this perfectly. For example when a body moves through still air, distant parts of the air have uniform velocity ($0ms^{-1}$) meaning there is no horizontal pressure gradient. However in a wind tunnel the distant parts of the fluid do not have the same velocities, due to the walls of the wind tunnel creating turbulence, therefore the horizontal

pressure gradient is not zero. In this case “there is a horizontal buoyancy to be applied as a correction” [30].

This horizontal buoyancy effect creates more drag on the wind tunnel model than it would experience moving through still air. This extra drag is known as the pressure-drop drag and is given by equation 4.3.

$$R = av \quad (equation\ 4.3\ [30])$$

Where R is the pressure-drop drag, a is the pressure gradient along the wind tunnel (constant in most wind tunnels) and v is the volume of the model. This extra drag force measured in a wind tunnel would give a larger drag coefficient than would be experienced in the real world. The effect of horizontal buoyancy and the boundary layer found in the wind tunnel mean that the coefficient of drag of the concept car found in the wind tunnel would be different if it were moving through still air.

5 Sustainability

Current scientific consensus suggests that artificial climate change is happening. In 2013, for example,of 10,885 peer reviewed climate articles only 2 rejected artificial climate change [31]. The IPCC state that even if all greenhouse gas emissions were halted immediately, "a scenario that is not plausible", global temperatures would still rise by 0.6°C by the end of the century [32]. This rising global temperature will lead to increased frequency, intensity and duration of weather events such as; heavy rainfall, drought and intense storm surges. Considering sustainability in any project is therefore of upmost importance. This section discusses the sustainability of certain aspects of this project.

5.1 Automotive Drag force

One aim of this project was to measure the drag force of a concept car in a wind tunnel. This practise is performed regularly when reducing the drag coefficient of cars. This drag coefficient, as explained in section 2.2, has a direct affect on fuel consumption. In general a 2% reduction in aerodynamic drag translates to a 1% reduction in fuel consumption [33]. A reduction in fuel consumption is important given that fossil fuels, such as Diesel and Petrol, are not renewable.

This reduction in fuel consumption due to a reduction in drag leads to a decrease in the greenhouse gas emissions from a car. A reduction in greenhouse gas emissions, particularly CO_2, is very important in order to slow the consequences of artificial climate change. The bulk of automotive greenhouse emissions occur along linear sources of pollution, such as motorways [34]. In this case cars are travelling at around 70mph and are not accelerating or decelerating excessively, therefore the main source of resistance is aerodynamic drag meaning that a reduction in drag would cause a large reduction in emissions. This is why the drag coefficient of a car is an important sustainability aspect.

5.2 Wind Tunnel vs CFD Energy Use

By replacing some physical wind tunnel testing with CFD simulation an energy saving could be made in the design process. Below is an assessment of how the energy consumption of a wind tunnel compares to CFD.

An industrial sized wind tunnel facility for use by a large automotive company can draw 6180kW of power for the fans [35]. Most modern computers tend to perform around $1x10^{16}$ computations per kWh [36], this value is increasing by Koomey's law [37], meaning the energy efficiency of computers approximately doubles every year and a half. Therefore currently a computer can run around $6.18x10^{19}$ computations for the same power consumption as an hour of industrial sized wind tunnel testing.

Clearly computational analysis is far more energy efficient than physical wind tunnel testing and is only becoming more energy efficient as technology advances. Therefore the automotive design process would be far more energy efficient and sustainable if it were to replace as much physical wind tunnel testing with CFD as possible.

6 Future Work

This section gives details about future work to improve the experimental results and the wind tunnel test section by adding new features which could be useful for further experimentation.

6.1 Further Experimental Testing

To improve the accuracy of the results found by the drag balance the tests could be repeated. Unfortunately repeat tests were not able to be performed in this case as the ALM printed concept car model was accidentally broken by an outside party. If the concept car model could be replaced the tests could be repeated and the results compared to check their accuracy.

6.2 Smoke Visualisation/Ventilation

Currently there is no form of flow visualisation in the wind tunnel test section. The properties of the flow have to be inferred from measurements taken by instruments such as pitot tubes. One common way of viewing flows in wind tunnels is by injecting smoke into the stream. This smoke forms streaklines which show up in contrast to the walls of the wind tunnel. These streaklines give a picture of the position of the particles which have passed through the point at which the smoke is injected [7]. These streaklines can be filmed (often in conjunction with a strobe light) or photographed to visualise the flow. They could also be filmed stereoscopically, this technique is described further in section 6.3.

In order to use smoke as a form of visualisation it must be removed from the flow at the exit of the wind tunnel, if this isn't done then the room in which the wind tunnel is operating will fill up with smoke; decreasing visibility and becoming a health and safety issue. Therefore the smoke needs to be ventilated outside. This could be done either by rearranging the layout of the room and having the exit of the wind tunnel feed directly outside or by attaching a flexible pipe to the exit of the wind tunnel which feeds into the existing extraction systems.

6.3 Stereoscopic Visualisation

Once the smoke ventilation is achieved the next issue is to determine the best way of viewing and recording imagery of the smoke in the flow. Given that the flow around the model is three dimensional it may be appropriate to capture images in three dimensions as opposed to just filming it in two. To achieve this stereoscopy could be used.

Stereoscopy is the process of giving the illusion of 3-D depth from a 2-D image. This is done by the process of stereopsis. Stereopsis is the ability of the human brain to "receive slightly different images from each eye, discrepant images, and then fuse them into a single image that has depth" [38]. This is achieved by projecting different images into the left and right eye, usually by projecting the two images on top of each other polarised differently. The viewer wears polarised glasses such that the left image is viewed by the left eye (the right image is omitted) and the right image is viewed by the right eye (the left image is omitted). To achieve this, two images must be taken from different points of view. Effectively the two cameras imitate the positioning of the human eyes, one recording what the left eye sees and one recording the right.

Given that the design of the test section includes a large glass window in the front, there is potential to fix a camera rig to the front of the test section to record the inside stereoscopically. This could output two images/videos of the flow inside the wind tunnel which could be converted into a ‘3-D’ image/video and used for flow analysis and presentation purposes.

6.4 Alternative Equipment

One final future improvement to the wind tunnel test section would be to invest in some new or alternative equipment. Ideally some testing would have been performed with a hot-wire anemometer, however the available probe was broken. Performing future experiments with a hot-wire probe could prove useful as a comparison to the pitot tube measurements making experimental testing more accurate. In order to achieve this a new hot-wire probe would need to be purchased, a typical example costing £232 [39].

Other useful future investments to improve the accuracy of results gained in the wind tunnel could be more precise load meters. Better quality load cells and force meters than the ones used for this experimentation are available, the cost of these instruments was unable to be justified for this project given the limited budget however if the investment could be found these meters could quickly and easily be installed in the drag balance and give more precise results. The precision of these meters could be fine enough to find the frictional forces mentioned in section 4.2.3 and they could be taken into account.

7 Conclusion

This report described the process and results of wind tunnel experimentation on a concept car. These results were to be compared with equivalent CFD simulations. In order to find accurate experimental results the wind tunnel test section had to be redesigned, the design of which was informed from experience gained using the previous test section to test the drag force on a cylinder. This test section was then manufactured and installed in an open-circuit wind tunnel and used for experimentation to find the drag coefficient of a concept car. Finally the report described some of the sustainability aspects of the project.

The wind tunnel test section built for this project can be used for many future experiments. The in-built drag balance and probe movement mechanism can be used for many testing applications, they are not limited to automotive tests. The test section was designed such that any future work into flow visualisation could be easily incorporated.

The coefficient of drag found by the experimentation was 0.17 ± 0.015. The comparable CFD setup gave the coefficient of drag to be 0.167. This shows that a 'virtual wind tunnel' produced using CFD is a valid counterpart to physical wind tunnel testing and that its use in the automotive design process is appropriate. CFD, as a parallel to physical wind tunnel testing , can therefore be used in automotive design, the advantages being that CFD is more sustainable and that CFD can test many different iterations of a design in a far shorter time than physical wind tunnel testing. Therefore an appropriate use of CFD in the automotive design process would be to test many different iterations of a design, finding the optimal one, before testing this design physically. Furthermore CFD can be used to test car designs in a range of different environments and flow conditions far cheaper and faster than physical wind tunnel testing.

8 References

[1] Pankhurst, R. C, Holder, D.W. (1952) *Wind-Tunnel Technique*. London: Sir Isaac Pitman & Sons Ltd

[2] Docherty, D. (2013) *Virtual Wind Tunnel Individual Report I1*. Exeter: University of Exeter.

[3] Perspex Distribution Ltd. (2014) *Perspex Cast Acrylic*. [Online] Available: perspex.co.uk

[4] European Commission. (2014) *Reducing CO2 from Passenger Cars*. [Online] Available: ec.europa.eu/clima/policies/transport/vehicles/cars/index_en.htm

[5] Risch-Janson, M. (2007) *Gas Mileage Dependance on Area and Drag Coefficient*. Minnesota: College of Saint Benedict and Saint John's University.

[6] Browand, F. (2005) *Reducing Aerodynamic Drag and Fuel Consumption*. California: Stanford University

[7] Douglas, J.F, Gasiorek, J.M, Swaffield, J.A. (1979) *Fluid Mechanics*. London: Pitman Publishing.

[8] Huebsch, B.R, Munson, B.R, Okiishi, T.H, Young, D.F. (2011) *A Brief Introduction to Fluid Mechanics*. Massachusetts: John Wiley & Sons, Inc.

[9] The Telegraph (2014) *The best-selling cars of 2013*. [Online] Available: telegraph.co.uk/motoring/picturegalleries/10530408/The-best-selling-cars-of-2013.html?frame=2556129

[10] EcoModder (2013) *Vehicle Coefficient of Drag List*. [Online] Available:

ecomodder.com/wiki/index.php/Vehicle_Coefficient_of_Drag_List

[11] White, F. M. (1986) *Fluid Mechanics*. New York: McGraw-Hill.

[12] Blades, L. (2014). *Individual Report I2: Virtual Wind Tunnel Project.* MEng Report. University of Exeter

[13] Lerner, L. S. (1996). *Modern Physics for Scientists and Engineers*. London: Jones and Bartlett Publishers Inc.

[14] TD Models & Scientific Co. (2010) *Newton Meters*. [Online] Available: tdmodelsindia.net/newton-meters.htm

[15] Jouaneh, M. (2013). *Fundamentals of Mechatronics*. Stamford: Cengage Learning

[16] Cerulean. (2010). *Arduino and Load Cell*. [Online] Available: cerulean.dk/words/?page_id=42

[17] Pope, E. J. (1997) *Rules of Thumb for Mechanical Engineers*. Gulf Publishing co. Texas.

[18] Ghosh, A. K. (2009). *Introduction to Measurements and Instrumentation*. PHI Learning Private Ltd, New Delhi

[19] eFunda. (2014) *Sensitivity of Strain Gage Wire Materials*. [Online] Available: efunda.com/designstandards/sensors/strain_gages/strain_gage_sensitivity

[20] Hangzhou Loadcell Electric Manufacturing Co.,Ltd. (2014) S-Beam Load Cell. [Online] Available: www.chinaloadcells.com/pid13173156/S21Y+S-Beam+Load+Cell(25kg~30000kg).htm

[21] Eren, H. & Webster, J. G. (2014) *Measurement, Instrumentation, and Sensors Handbook: Spatial, Mechanical, Thermal, and Radiation Measurement*. Florida: Taylor & Francis Group.

[22] Browne, F. (2014). *Individual Report I2: Virtual Wind Tunnel Project.* MEng Report. University of Exeter.

[23] University of Waterloo. (1997) *Fluid Properties Calculator*. [Online] Available: mhtl.uwaterloo.ca/old/onlinetools/airprop/airprop.html

[24] Dassault Systèmes, Solidworks (Version 2014) [Computer program]

[25] Nima, D. (2014). *Individual Report I2: Virtual Wind Tunnel Project.* MEng Report. University of Exeter

[26] ANSYS, Inc., ANSYS FLUENT (Version 14.5) [Computer program]

[27] Hong, P. (2011) *2012 BMW 328i*. [Online] Available: roadandtrack.com/car-reviews/first-drives/2012-bmw-328i

[28] Engineering Toolbox. (2014) *Air – Absolute and Kinematic Viscosity*. [Online] Available: engineeringtoolbox.com/air-absolute-kinematic-viscosity-d_601.html

[29] Kothandaraman, C. P, & Rudramoorthy, R (1999) *Basic Fluid Mechanics*. New Delhi: New Age International Ltd.

[30] Zahn, A. F. (1920) *Horizontal Buoyancy in Wind Tunnels: Technical Note No.23*. USA: National Advisory Committee for Aeronautics

[31] Powell, J. L. (2014) *Science and Global Warming*. [Online] Available: jamespowell.org

[32] Collins, M. & Knutti, R. (2013) Chapter 12: Long Term Climate Change: Projections, Commitments and Irreversibility. In *Climate Change 2013: The Physical Science Basis*. Intercontinental Panel on Climate Change.

[33] Clinger, J. Douglass, K. Kasper, D. Mastroianni, S. & Yassitepe, E. (2009) *Carbon Emissions Reduction via Increased Fuel Economy*. Delaware: University of Delaware

[34] Civis, M., Hinson, A. V., Pederson, K. & Przychodzka, M. (2003) *Environmental Impact Assessment of Petrol Usage*. University of Aarhus: Centre for Environmental Studies.

[35] BMW. (2012) *Innovation Days Efficient Dynamics: Energy and Environmental Test Centre*. [Online] Available: multimedia.jp.dk/archive/00265/bmw-vindtunnel_265613a.pdf

[36] Reams, C. (2012) *Modelling energy efficiency for computation*. Cambridge: University of Cambridge Computer Laboratory.

[37] Gangadharan, G. R. & Murugesan, S. (2012) *Harnessing Green IT: Principles and Practices*. Chichester: John Wiley and Sons Ltd.

[38] Curry, T. S, Dowdey, J. E. & Murry, R. C. (1990). *Christensen's Physics of Diagnostic Radiology*. Pennsylvania: Lippincott Williams & Wilkins.

[39] Dantec Dynamics. (2014) *Cable-equipped wire probe*. [Online] Available:dantecdynamics.com/cable-equipped-wire-probe